This full text paper was peer reviewed at the direction of IEEE Communications Society subject matter experts for publication in the IEEE Globecom 2010 proceedings.

Channel inversion in MIMO systems over Rician fading

Damith Senaratne and Chintha Tellambura
Department of Electrical and Computer Engineering,
University of Alberta, Edmonton, AB, Canada.
Email: {damith,chintha}@ece.ualberta.ca

Himal A. Suraweera
Department of Electrical and Computer Engineering,
National University of Singapore, Singapore.
Email: elesaha@nus.edu.sg

***Abstract*—We examine the distribution of the per virtual-channel received signal-to-noise ratio over a multiple-input multiple-output channel modeled by a rank-2 non-central Wishart matrix. The exact probability density function is derived for all possible non-centrality matrices; and verified through simulation for selected systems. Identities for exact analytic results on the outage probability, the average symbol error rate, and the moment generating function are also derived.**

***Index Terms*—MIMO, channel inversion, non-central Wishart distribution, outage probability, symbol error rate.**

I. Introduction

A multiple-input multiple-output (MIMO) system [1] with N_t transmit antennas and N_r receive antennas is modeled by an $N_r \times N_t$ 'channel matrix'. With perfect transmit channel-state-information, the transmit precoding and receiver reconstruction matrices can be chosen such that the channel reduces to a set of eigenmodes that can be independently coded, modulated, and power allocated for.

Channel Inversion [2] power allocation scheme seeks to maintain the per-channel instantaneous received signal-to-noise ratio (SNR) identical, and the total instantaneous transmit power a constant all the time. In other words, it causes power $p_i, i = 1 \dots n$ to be allocated for the channels having respective instantaneous gains λ_i so that $\sum_{\forall i} p_i = P$ is constant; and $\lambda_i p_i$ identical across the channels $i = 1 \dots n$. Channel-inversion is capacity-wise inferior to the classical water-filling power allocation scheme. Yet, it is unique among the power allocation schemes in assuring the fairness across the channels with respect to achievable capacity.

Channel-inversion has further advantages in the MIMO context[1] [4]–[6]. It is implementable with non-iterative transmitter processing and unitary receiver processing [4], [6]. Hence, no noise enhancement occurs at the receiver. When the channel rank is limited by the number of receiver antennas, receiver processing is not required at all; and the resulting virtual channels correspond one-to-one with the receiver antennas. This, makes channel-inversion suitable for multi-user MIMO downlink channels [7]. References [8]–[10] examine variants of channel inversion that seek to improve the capacity.

[1] 'Zero forcing' at the transmitter [3] too inverts the channel. It maintains the per virtual-channel received power and the average transmit power steady. On the other hand channel inversion, being a power allocation scheme, keeps the total instantaneous transmit power steady, and the instantaneous per virtual-channel received power identical.

Analyzing MIMO channels in fading requires results from random matrix theory [11]. The eigenmodes of a MIMO channel comprising independent and identically distributed Rayleigh faded transmit-receive links, for instance, have the gains governed by the eigenvalue distribution associated with the Central Wishart distribution [12]. Similarly, non-central Wishart Distribution corresponds to Rician fading, which arises owing to line-of-sight conditions [13].

This work generalizes [14] on Rayleigh fading, including it in the case the non-centrality matrix has both eigenvalues zero. The exact probability density function (pdf) of a factor proportional to per virtual-channel received SNR is derived, for non-central Wishart matrices of order $n \geq 2$ having rank-2. All possible non-centrality matrices are considered. The pdf result is then used to derive important performance metrics including the outage probability, and the average symbol error rate. The moment generating function too is derived. All required identities are proven here even though some expressions are omitted for brevity. To further the insights, the first order approximation of the pdf characterizing the high SNR behavior is also provided.

The paper is organized as follows: Sections II and III present the system model and the mathematical formulation. Section IV highlights how certain performance metrics can be obtained. In Section V, the results are verified for selected MIMO configurations through Monte-Carlo simulation. Section VI concludes the paper. Proof of Theorem 1 is annexed.

Notation: $P[\cdot]$ is the *probability assignment*; and $\mathcal{E}_\Lambda\{\cdot\}$ is the *expectation operator* with respect to a random variable Λ. The pdf, the cumulative distribution function (cdf) and the moment generating function (mgf) of Λ are given by $f_\Lambda(\cdot)$, $F_\Lambda(\cdot)$ and $\mathcal{M}_\Lambda(\cdot)$ respectively. $\mathbb{C}^{n,m}$ represents the space spanned by $n \times m$ complex Gaussian matrices. $(\cdot)^H$ and $||\cdot||_F$ designate the conjugate transpose and the Frobenius norm of a matrix. $\text{eig}(\cdot)$ yields the eigenvalues of a square matrix.

Modified Bessel Functions of the First Kind and *the Second Kind* [15, 9.6] having order ν are denoted by $\mathcal{I}_\nu(\cdot)$ and $\mathcal{K}_\nu(\cdot)$ respectively. $\mathcal{Q}(\cdot)$ represents the *Gaussian Q-function* [15, Eq. (26.2.3)], while $\Gamma(\cdot)$ denotes the Gamma function [15, 6.1]. $\mathcal{G}_{p\ q}^{m\ n}\left(\cdot \,\middle|\, \begin{matrix} a_1, \dots, a_n, a_{n+1}, \dots, a_p \\ b_1, \dots, b_m, b_{m+1}, \dots, b_q \end{matrix}\right)$ represents the *Meijer G function* [16, p.419]. $\mathcal{L}\{\cdot\}$ is the Laplace Transform.

978-1-4244-5638-3/10/$26.00 ©2010 IEEE

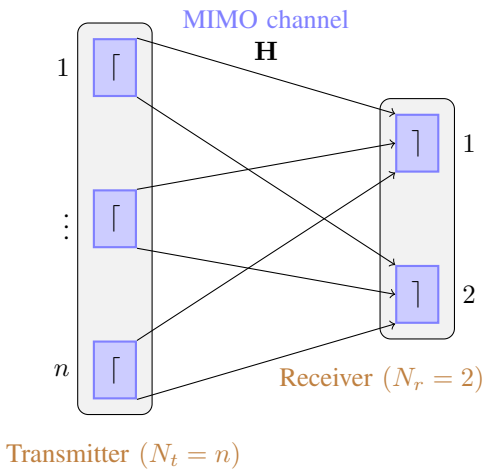

Fig. 1. System Model: A MIMO channel between a transmitter having $n \geq 2$ antennas, and a receiver having 2 antennas. The line-of-sight paths are indicated; while isotropic scattering is assumed. The results also hold in the reverse direction for $N_t = 2, N_r = n$.

II. System Model

Consider a MIMO system having N_t transmit antennas and N_r receive antennas, where $\min(N_t, N_r) = 2$ (see Fig. 1). Let $n = \max(N_t, N_r) \geq 2$. This scenario can occur in any MIMO channel with 2 antennas at one end; and at least 2 antennas in the other. It occurs even in certain multiuser MIMO configurations, such as in the downlink channel from a multi-antenna base station to two single-antenna mobile stations it simultaneously communicates with.

Without further loss of generality let $N_t = n$ and $N_r = 2$. Suppose the $2 \times n$ channel matrix $\mathbf{H}$ is of form

$$\mathbf{H} = a\mathbf{H}_{\text{sp}} + b\mathbf{H}_{\text{sc}}, \tag{1}$$

where $\mathbf{H}_{\text{sp}}$ is a deterministic specular (line-of-sight) component, $\mathbf{H}_{\text{sc}} \in \mathbb{C}^{2,n}$ a random scatter component, and $a^2 + b^2 = 1$. The specular component is governed by the directional gains of the antennas, presence of dominant multi-paths, etc. $K = \frac{a^2||\mathbf{H}_{\text{sp}}||_F^2}{b^2||\mathbf{H}_{\text{sc}}||_F^2}$ gives the Rician factor [17]. $\mathbf{\Omega} = \frac{a^2}{b^2}\mathbf{H}_{\text{sp}}\mathbf{H}_{\text{sp}}^H$ is the 'non-centrality matrix'.

Let, $\{\lambda_1, \lambda_2\} = \text{eig}\left(\mathbf{H}\mathbf{H}^H\right)$ and $\{\omega_1, \omega_2 | \omega_1 > \omega_2\} = \text{eig}\left(\mathbf{\Omega}\right)$. The joint distribution of unordered eigenvalues is given by [17, Eq. (15)]

$$\begin{aligned} f_{\lambda_1,\lambda_2}(\lambda_1, \lambda_2) = \frac{\mathrm{e}^{-(\omega_1+\omega_2)}}{2} \frac{(\lambda_1 - \lambda_2)(\lambda_1\lambda_2)^{\frac{n-2}{2}}}{(\omega_1 - \omega_2)(\omega_1\omega_2)^{\frac{n-2}{2}}} \\ \mathrm{e}^{-(\lambda_1+\lambda_2)} \left(\mathcal{I}_{n-2}\left(2\sqrt{\omega_1\lambda_1}\right)\mathcal{I}_{n-2}\left(2\sqrt{\omega_2\lambda_2}\right)\right. \\ \left. -\mathcal{I}_{n-2}\left(2\sqrt{\omega_2\lambda_1}\right)\mathcal{I}_{n-2}\left(2\sqrt{\omega_1\lambda_2}\right)\right). \end{aligned} \tag{2}$$

The specular component too being continuously distributed, the case $\omega_1 = \omega_2$ is not likely in practice. However, it can occur with non-zero probability in the model since $\mathbf{H}_{sp}$ is considered to be deterministic. Corresponding pdf is given by the limiting operation $\omega_1 \to \omega_2$ on (2).

Assume perfect transmit CSI, and the channel inversion power allocation scheme. Given total transmit SNR $\bar{\gamma}_0$, per channel received SNR is given by $\frac{b^2}{2}\bar{\gamma}_0\Lambda$, where

$$\Lambda = \frac{\lambda_1\lambda_2}{\lambda_1 + \lambda_2}. \tag{3}$$

In this paper, we will present new exact outage probability and SER results for the channel (1). The major mathematical challenge in establishing them is deriving the statistical distribution of Λ.

III. Mathematical Formulation

Theorem 1: the pdf of Λ
Let λ_1, λ_2 be the eigenvalues of a rank-2 non-central complex Wishart matrix having n degrees of freedom, and non-centrality matrix Ω whose eigenvalues are $\{\omega_1, \omega_2 | \omega_1 \geq \omega_2 > 0\}$. The pdf of Λ in (3) is given by:

$$\begin{aligned} f_\Lambda(x) = \sum_{i=0}^{\infty}\sum_{j=0}^{i} \frac{g_{j,(i-j)}(\omega_1, \omega_2)}{(j+n-2)!\,(i-j+n-2)!\,j!\,(i-j)!} \\ \sum_{p=0}^{i+2n-1} \binom{i+2n-1}{p} \mathrm{e}^{-2x} x^{i+2n-2} \\ \left(\mathcal{K}_{n+j-p}(2x) - \mathcal{K}_{n+j-p-1}(2x)\right), \end{aligned} \tag{4}$$

where

$$g_{i,j}(\alpha, \beta) = \begin{cases} \frac{\mathrm{e}^{-(\alpha+\beta)}}{(\alpha-\beta)}\left(\alpha^i\beta^j - \alpha^j\beta^i\right), & \alpha \neq \beta \\ (i-j)\alpha^{i+j-1}\mathrm{e}^{-2\alpha}, & \alpha = \beta \end{cases}. \tag{5}$$

Proof: See Appendix. ■

When the non-centrality matrix has one non-zero eigenvalue (i.e. $\omega_1 \neq 0, \omega_2 = 0$), $g_{j,(i-j)}(\omega_1, \omega_2)$ in (4) is non-zero only when $(j = 0, i \neq j)$ or $(j \neq 0, i = j)$. Thus the pdf simplifies as follows.

Corollary 1:
Let λ_1, λ_2 be the eigenvalues of a rank-2 non-central complex Wishart matrix having n degrees of freedom, and non-centrality matrix Ω whose eigenvalues are $\{\omega_1, \omega_2 | \omega_1 > 0, \omega_2 = 0\}$. The pdf of Λ in (3) is given by:

$$\begin{aligned} f_\Lambda(x) = \sum_{i=1}^{\infty} \frac{\omega_1^{i-1}\mathrm{e}^{-\omega_1}}{(n-2)!\,(i+n-2)!\,i!} \\ \sum_{p=0}^{i+2n-1} \binom{i+2n-1}{p} \mathrm{e}^{-2x} x^{i+2n-2} \\ \left(\mathcal{K}_{n+i-p}(2x) - \mathcal{K}_{n-p}(2x)\right. \\ \left. -\mathcal{K}_{n+i-p-1}(2x) + \mathcal{K}_{n-p-1}(2x)\right) \end{aligned} \tag{6}$$

Proof: Omitted. ■

Setting $\omega_1 = 0$ in (6) yields (7), which is identical to the pdf of corresponding central Wishart distribution (i.e. Rayligh fading). Its equivalence to [14, Thm. 1] can be easily established using [18, Eq. (3.4.17.5.1)].

$$\begin{aligned} f_\Lambda(x) = \frac{1}{(n-2)!\,(n-1)!} \sum_{p=0}^{2n} \binom{2n}{p} \mathrm{e}^{-2x} x^{2n-1} \\ \left(\mathcal{K}_{n-p+1}(2x) - 2\mathcal{K}_{n-p}(2x) + \mathcal{K}_{n-p-1}(2x)\right) \end{aligned} \tag{7}$$

IV. Applications

The pdf $f_\Lambda(x)$ expressions given by (4), (6) or (7) allow performance metrics such as the outage probability to be derived. Required identities are proven here.

A. Outage Probability

An outage occurs when the instantaneous received SNR falls below an acceptable SNR threshold γ_{th}. Hence, its probability, i.e. the 'outage probability', can be given in terms of the cdf $F_\Lambda(x) = \int_0^x f_\Lambda(t)\,\mathrm{d}t$, which reduces to be a weighted sum of integrals of the form $\int_0^x t^\mu \mathrm{e}^{-2t}\mathcal{K}_\nu(2t)\,\mathrm{d}t$. It may be simplified as follows using the identities [19, 9.34.4], and [18, Eq. (7.34.21.2.1)].

$$\begin{aligned}\int_0^x t^\mu \mathrm{e}^{-2t}\mathcal{K}_\nu(2t)\,\mathrm{d}t &= \sqrt{\pi}\int_0^x t^\mu \mathcal{G}_{1\ 2}^{2\ 0}\left(4t\,\middle|\,\begin{matrix}0.5\\ \nu,-\nu\end{matrix}\right)\mathrm{d}t\\ &= \frac{\sqrt{\pi}}{4^{\mu+1}}\int_0^{4x} t^\mu \mathcal{G}_{1\ 2}^{2\ 0}\left(t\,\middle|\,\begin{matrix}0.5\\ \nu,-\nu\end{matrix}\right)\mathrm{d}t\\ &= \frac{\sqrt{\pi}}{4^{\mu+1}}\mathcal{G}_{2\ 3}^{2\ 1}\left(4x\,\middle|\,\begin{matrix}1,\ \mu+1.5\\ \mu+\nu+1,\ \mu-\nu+1,\ 0\end{matrix}\right) \qquad (8)\end{aligned}$$

The Meijer G function is available in popular computational software such as MATLAB, Maple and Mathematica.

B. Average Symbol Error Rate

The SER is the probability a transmitted symbol is incorrectly decoded at the receiver. It is dependent on the instantaneous channel-state; the 'average SER' obtained through averaging over all possible channel-states characterizes the overall quality of the channel. Under many modulation schemes this can be represented or approximated as $\mathcal{E}_\Lambda\{\alpha\mathcal{Q}\left(\sqrt{2\beta\Lambda}\right)\}$. This, given by $\frac{\alpha}{2}\sqrt{\frac{\beta}{\pi}}\int_0^\infty \frac{\mathrm{e}^{-\beta t}}{\sqrt{t}}F_\Lambda(t)\,\mathrm{d}t$, is a weighted sum of integrals of the form $\int_0^\infty t^{-0.5}\mathrm{e}^{-\beta t}\mathcal{G}_{2\ 3}^{2\ 1}\left(4t\,\middle|\,\begin{matrix}1,\ \rho\\ \mu,\ \nu,\ 0\end{matrix}\right)\mathrm{d}t$. Further simplification is possible using [18, Eq. (7.34.22.3.1)].

$$\begin{aligned}&\int_0^\infty t^{-0.5}\mathrm{e}^{-\beta t}\mathcal{G}_{2\ 3}^{2\ 1}\left(4t\,\middle|\,\begin{matrix}1,\ \rho\\ \mu,\ \nu,\ 0\end{matrix}\right)\mathrm{d}t\\ &\quad= \mathcal{L}\left\{t^{-0.5}\mathcal{G}_{2\ 3}^{2\ 1}\left(4t\,\middle|\,\begin{matrix}1,\ \rho\\ \mu,\ \nu,\ 0\end{matrix}\right)\right\}\Big|_{s\doteq\beta}\\ &\quad= \beta^{-0.5}\mathcal{G}_{3\ 3}^{2\ 2}\left(\frac{4}{\beta}\,\middle|\,\begin{matrix}0.5,\ 1,\ \rho\\ \mu,\ \nu,\ 0\end{matrix}\right) \qquad (9)\end{aligned}$$

C. Moment Generating Function

Similarly, the mgf of Λ, defined as $\mathcal{E}_\Lambda\{\mathrm{e}^{-s\Lambda}\} = \frac{1}{s}\int_0^\infty \mathrm{e}^{-st}F_\Lambda(t)\,\mathrm{d}t$, can be obtained [18, Eq. (7.34.22.3.1)] as a weighted sum of terms of form

$$\int_0^\infty \frac{\mathrm{e}^{-st}}{s}\mathcal{G}_{2\ 3}^{2\ 1}\left(4t\,\middle|\,\begin{matrix}1,\ \rho\\ \mu,\ \nu,\ 0\end{matrix}\right)\mathrm{d}t = \frac{1}{s}\mathcal{G}_{3\ 3}^{2\ 2}\left(\frac{4}{s}\,\middle|\,\begin{matrix}0,\ 1,\ \rho\\ \mu,\ \nu,\ 0\end{matrix}\right). \qquad (10)$$

The mgf itself is not a performance metric[2]. Its importance lies mainly in the fact that the mgf is a starting point for computing many numerical performance results.

[2]Incidentally, the mgf result gives the exact symbol error rate for differential phase shift keying modulation scheme.

D. Diversity Order

The pdf result is a weighted sum of $\mathrm{e}^{-2x}x^\mu\mathcal{K}_\nu(2x)$ terms. Using [15, Eq. (9.6.9)], and with some manipulations, the first order approximation of (4) can be obtained.

Corollary 2:
Let λ_1, λ_2 be the eigenvalues of a rank-2 non-central complex Wishart matrix having n degrees of freedom, and non-centrality matrix Ω whose eigenvalues are $\{\omega_1, \omega_2 | \omega_1 \geq \omega_2 > 0\}$. The first order approximation of the pdf of Λ in (3) given by $f_\Lambda(x) \approx ax^{n-2}$, where

$$a = \begin{cases}\frac{\mathrm{e}^{-\omega_1}}{2}\frac{(n+\omega_1)}{(n-2)!}, & \omega_1 = \omega_2 > 0\\ \frac{(n-1+\omega_1)\mathrm{e}^{-\omega_2}-(n+\omega_2-1)\mathrm{e}^{-\omega_1}}{2(\omega_1-\omega_2)}\frac{}{(n-2)!}, & \omega_1 > \omega_2 > 0\end{cases}. \qquad (11)$$

Proof: Omitted. ∎

The above is sufficient to derive the diversity order and the coding gain [20]. Diversity order is $(n-1)$, as would have been with zero-forcing [21]. Similar results can be computed for (6) and (7).

V. Numerical Results

Figures 2 through 5 verify the analytical results, for selected MIMO configurations, via semi-analytic Monte-Carlo simulation (conducted with 10^6 simulation points).

Fig. 2 corresponds to rank-2 non-centrality matrices having unequal eigenvalues $(\omega_1 = 4, \omega_2 = 1)$. Close agreement of analytic and simulation results supports the proof to establish the validity of (4). Although not as evident with the cdf or average SER, near-zero behavior of a pdf curve (i.e. $\lim_{x\to 0} f_\Lambda(x)$), reflects the diversity order. Reaffirming the results derived in Section IV-D, the pdf curves for larger n slope downward more rapidly, at the vicinity of $x = 0$.

A non-centrality matrix having all zero eigenvalues need not be a zero matrix. But a zero matrix always has all eigenvalues zero. Therefore (7) is identical to what already derived and verified for Rayleigh fading in [14, Thm. 1].

The cdf result for non-centrality matrices having unequal eigenvalues $(\omega_1 = 4, \omega_2 = 1)$ is shown in Fig. 3. Shown in dotted lines are the curves corresponding to case $(\omega_1 = 0, \omega_2 = 0)$, which encompasses the Rayleigh fading scenario. It highlights the fact that the presence of a specular component improves the outage probability. The increase of the diversity order with n is apparent in the slope of the cdf as $x \to 0$, which is the slope of the outage curve as normalized equivalent SNR tends to infinity.

Fig. 4 depicts the average SER for binary phase shift keying (BPSK) modulation, for a 2×3 MIMO system, and a non-centrality matrix given by $(\omega_1 = 6 \times 10^{K/10}, \omega_2 = 0)$, thereby indirectly establishing the validity of (6). K is the Rician factor in dB. The rank-1 non-centrality matrix of this case arises from directional gain of the transmit and receive antenna arrays [17]. Corresponding curve for the Rayleigh fading scenario is also given. The fact that increasing the Rician factor K improves the error performance can clearly be seen.

Fig. 5 shows the average SER for BPSK modulation, for the case $(\omega_1 = \omega_2 = 1)$. The asymptotic SER curves computed by

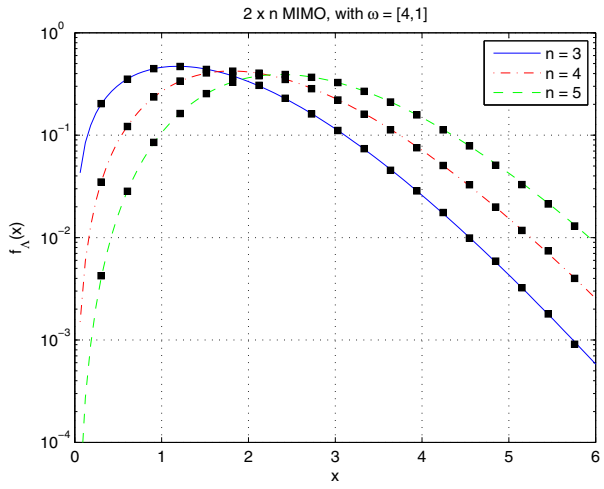

Fig. 2. The pdf, analytic vs. simulated (■), of Λ in (3) over a $2 \times n$ MIMO system, in Rician fading modeled by a rank-2 non-centrality matrix having eigenvalues $[4, 1]$.

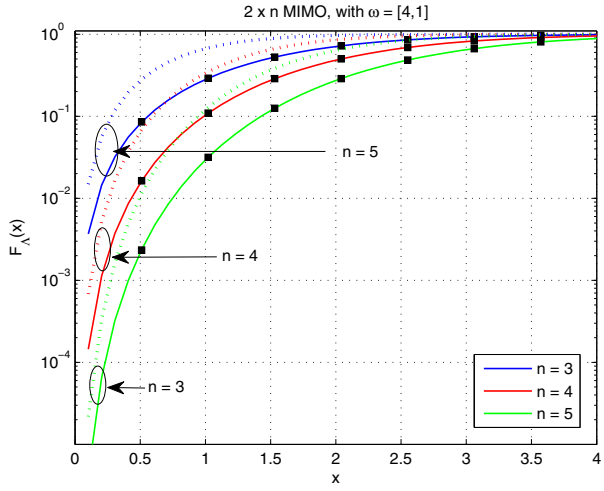

Fig. 3. The cdf, analytic (solid lines) vs. simulated (■), of Λ in (3) over a $2 \times n$ MIMO system, in Rician fading modeled by a rank-2 non-centrality matrix having eigenvalues $[4, 1]$. The cdf for Rayleigh fading is shown in dotted lines.

ϵ	x	i	
		(for $n = 2$)	(for $n = 4$)
1×10^{-3}	0.1	17	6
	1	18	9
	5	1	1
1×10^{-5}	0.1	20	9
	1	21	11
	5	1	12
1×10^{-10}	0.1	27	14
	1	28	16
	5	29	19
1×10^{-13}	0.1	30	17
	1	31	19
	5	33	22

TABLE I
VALUE OF i AT WHICH THE TERMS OF THE OUTER SUM OF (4) FALL BELOW $\epsilon \times \mathrm{e}^{-(\omega_1+\omega_2)}$ IN MAGNITUDE (FOR $\omega = [1, 4]$).

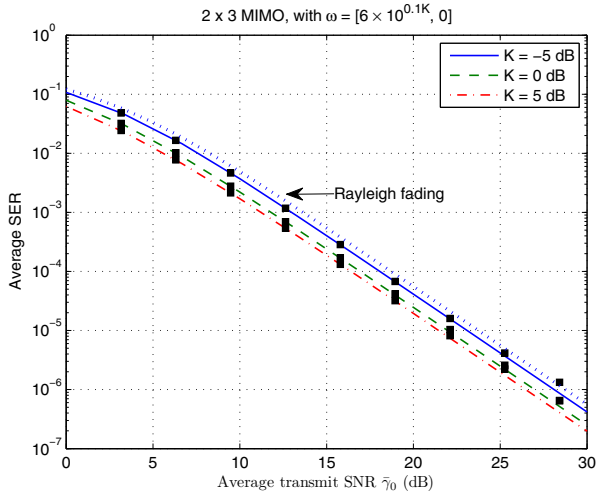

Fig. 4. The average SER for BPSK (i.e. $\alpha = 1, \beta = \frac{b^2}{2}\bar{\gamma}_0$), analytic vs. simulated (■), for a 2×3 MIMO system, in Rician fading modeled by a rank-1 non-centrality matrix parameterized [17] by $\{\theta_t = 20^o, \theta_r = 10^o, d = 1\}$.

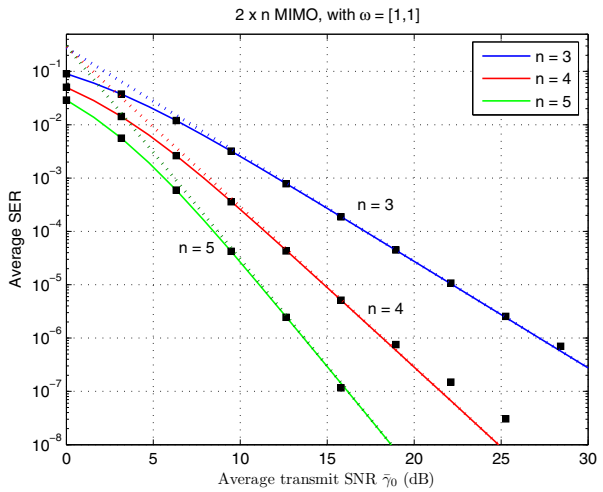

Fig. 5. The average SER for BPSK (i.e. $\alpha = 1, \beta = \frac{b^2}{2}\bar{\gamma}_0$), analytic (solid lines) vs. simulated (■), for a $2 \times n$ MIMO system, in Rician fading modeled by a rank-2 non-centrality matrix having equal eigenvalues of 1, for $b = \sqrt{2}$. Asymptotic SER curves are shown in dotted lines.

using (11) are shown in dotted lines. Diversity order, depicted by the asymptotic slope is seen increasing with n.

As each expression (4), (6) has an infinite summation, it is interesting to find out their rate of convergence, which determines their usefulness. Table I presents, for $(\omega_1 = 4, \omega_2 = 1)$ and six combinations of (n, x), the value of i beyond which the absolute value of the i^{th} term of (4) falls below a threshold $\epsilon \times \mathrm{e}^{-(\omega_1+\omega_2)}$. From Table I one can deduce that the convergence rate improves with n, and degrades with x. The observations deviating from this pattern (e.g. for $\epsilon = 10^{-3}, x = 5, n = 2$) are not unexpected; they arise when the first term of the sum itself is smaller than ϵ. However, the observations raise a concern. Convergence acceleration would be required for larger x and large Rician factors at higher precision.

978-1-4244-5638-3/10/$26.00 ©2010 IEEE

VI. Conclusion

The exact probability density result in [14] has been extended for the non-central Wishart scenario, for all forms of the non-centrality matrix. Identities that provide exact analytic results for the outage probability, the average SER, and others have been derived. The results were verified through Monte-Carlo simulation for selected configurations. Numerical results provide further insights on the effect of the Rician factor. Being associated with the distribution of the harmonic mean of the eigenvalues of a non-central Wishart matrix, the results could be useful for other applications as well.

VII. Appendix

Proof (Theorem 1): Let λ_1, λ_2 be the eigenvalues of a rank-2 non-central complex Wishart matrix having n degrees of freedom, and non-centrality matrix Ω having eigenvalues $\{\omega_1, \omega_2 | \omega_1 > \omega_2\}$. The joint pdf of λ_1, λ_2 is given by (2). Let $\Lambda = \frac{\lambda_1 \lambda_2}{\lambda_1 + \lambda_2}$.

$$\begin{aligned} \Rightarrow F_\Lambda(x) &= 1 - \int_x^\infty \bar{F}_{\lambda_2|\lambda_1}\left(\frac{\lambda_1 x}{\lambda_1 - x}\middle|\lambda_2\right) f_{\lambda_1}(\lambda_1)\,\mathrm{d}\lambda_1 \\ \therefore f_\Lambda(x) &= \int_0^\infty \frac{(t+x)^2}{t^2} f_{\lambda_1,\lambda_2}\left(t+x, \frac{x(t+x)}{t}\right)\mathrm{d}t \end{aligned}$$

Substituting from (2),

$$\begin{aligned} f_\Lambda(x) = \frac{\mathrm{e}^{-(\omega_1\omega_2)}}{2(\omega_1-\omega_2)(\omega_1\omega_2)^{\frac{n-2}{2}}} \\ \left(\mathbb{J}\left(\omega_1,\omega_2,\frac{n}{2},\frac{n}{2}-1\right) - \mathbb{J}\left(\omega_1,\omega_2,\frac{n}{2}-1,\frac{n}{2}\right)\right. \\ \left. -\mathbb{J}\left(\omega_2,\omega_1,\frac{n}{2},\frac{n}{2}-1\right) + \mathbb{J}\left(\omega_2,\omega_1,\frac{n}{2}-1,\frac{n}{2}\right)\right), \quad (12) \end{aligned}$$

where $$\mathbb{J}(a,b,k,l) = x^l \mathrm{e}^{-2x} \int_0^\infty \frac{(t+x)^{k+l-2}}{t^{l+2}}\,\mathrm{e}^{t+\frac{x^2}{t}} \mathcal{I}_{n-2}\left(2\sqrt{a(t+x)}\right)\mathcal{I}_{n-2}\left(2\sqrt{xb(t+x)}\right)\mathrm{d}t.$$

Using [15, 9.6.10], and then [19, 3.471(12)], we get

$$\begin{aligned} \mathbb{J}(a,b,k,l) = 2\mathrm{e}^{-2x} \sum_{i=0}^\infty \sum_{j=0}^i c_{j,i-j} \sum_{p=0}^{i+k+l+n} \\ \binom{i+k+l+n}{p} x^{i+k+l+n-1} \mathcal{K}_{n/2+j+k-p}(2x), \quad (13) \end{aligned}$$

where $c_{i,j} = \dfrac{a^{i+n/2-1} b^{j+n/2-1}}{(i+n-2)!\,(j+n-2)!\,i!\,j!}$.

Noting $a, b \in \{\omega_1, \omega_2\}$; $k, l \in \{n/2, n/2-1\}$; and $k+l = n-1$, Eqns. (12) and (13) can be simplified further, to obtain (4) where $g_{i,j}(\omega_1, \omega_2)$ is given by the case $\omega_1 \neq \omega_2$ of (5).

• Case: $\omega_1 = \omega_2$: Eqn. (2) does not hold as is when $\omega_1 = \omega_2$; but the limit $\omega_1 \to \omega_2$ does. Similarly, (4) holds true in the limiting form

$$\lim_{\omega_2 \to \omega_1} g_{i,j}(\omega_1, \omega_2) = \mathrm{e}^{-2\omega_1} \left(\lim_{\omega_2 \to \omega_1} \frac{\omega_1^i \omega_2^j - \omega_1^j \omega_2^i}{\omega_1 - \omega_2}\right).$$

We get the case $\omega_1 = \omega_2$ of (5) using the L'Hospital's rule. ■

Acknowledgment

This work is supported in part by the Alberta Ingenuity Fund through the iCORE ICT Graduate Student Award; and the Research Grant Numbers R-263-000-421-112 & R-263-000-436-112 of the National University of Singapore, Singapore.

References

[1] G. J. Foschini, "Layered space-time architecture for wireless communication in a fading environment when using multi-element antennas," *Bell Labs technical journal*, vol. 5, no. 2, pp. 41–59, 1996.

[2] A. J. Goldsmith and P. P. Varaiya, "Capacity of fading channels with channel side information," *IEEE Trans. Inf. Theory*, vol. 43, no. 6, pp. 1986–1992, Nov. 1997.

[3] R. U. Nabar, O. Oyman, H. Bölcskei, and A. J. Paulraj, "Capacity scaling laws in MIMO wireless networks," in *Proc. Allerton Conference on Communication, Control, and Computing*, Monticello, IL, Oct. 2003, pp. 378–389.

[4] T. Haustein, C. von Helmolt, E. Jorswieck, V. Jungnickel, and V. Pohl, "Performance of MIMO systems with channel inversion," in *Proc. IEEE Vehicular Technology Conference, VTC Spring*, Birmingham, AL, May 2002, pp. 35–39.

[5] E. Jorswieck, G. Wunder, V. Jungnickel, and T. Haustein, "Inverse eigenvalue statistics for Rayleigh and Rician MIMO channels," in *MIMO: Communications Systems from Concept to Implementations, IEE Seminar on*, Dec. 2001, pp. 1–3.

[6] V. Jungnickel, T. Haustein, E. Jorswieck, and C. von Helmolt, "A MIMO WLAN based on linear channel inversion," in *MIMO: Communications Systems from Concept to Implementations, IEE Seminar on*, Dec. 2001, pp. 1–20.

[7] H. Lee, K. Lee, B. M. Hochwald, and I. Lee, "Regularized channel inversion for multiple-antenna users in multiuser MIMO downlink," in *Proc. Communications, International Conference on*, Beijing, China, May 2008, pp. 3501–3505.

[8] V. Jungnickel, T. Haustein, V. Pohl, and C. von Helmolt, "Link adaptation in a multi-antenna system," in *Proc. Vehicular Technology Conference, VTC Spring*, vol. 2, Jeju, Korea, Apr. 2003, pp. 862–866.

[9] C. B. Peel, B. M. Hochwald, and A. L. Swindlehurst, "A vector-perturbation technique for near-capacity multiantenna multiuser communication-part I: channel inversion and regularization," *IEEE Trans. Commun.*, vol. 53, no. 1, pp. 195–202, Jan. 2005.

[10] C. Masouros and E. Alsusa, "Dynamic linear precoding for the exploitation of known interference in MIMO broadcast systems," *IEEE Trans. Wireless Commun.*, vol. 8, no. 3, pp. 1396–1404, Mar. 2009.

[11] A. M. Tulino and S. Verdu, *Random Matrix Theory and Wireless Communications*, 1st ed., ser. Foundations and Trends in Communications and Information Theory. Hanover, MA: now publishers, 2004, vol. 1.

[12] I. E. Telatar, "Capacity of multi-antenna Gaussian channels," Bell Laboratories, Lucent Technologies, Tech. Rep., Oct. 1995.

[13] J. Kermoal, L. Schumacher, K. Pedersen, P. Mogensen, and F. Frederiksen, "A stochastic MIMO radio channel model with experimental validation," *IEEE J. Sel. Areas Commun.*, vol. 20, no. 6, pp. 1211–1226, Aug. 2002.

[14] D. Senaratne and C. Tellambura, "Performance analysis of channel inversion over MIMO channels," in *Proc. IEEE Global Communication Conference*, Honolulu, HI, Dec. 2009.

[15] M. Abramowitz and I. Stegun, *Handbook of Mathematical Functions*. Dover Publications, Inc., New York, 1970.

[16] L. C. Andrews, *Special Functions of Mathematics for Engineers*, 2nd ed. New York, NY: McGraw-Hill, Inc., 1992.

[17] P. J. Smith and L. M. Garth, "Exact capacity distribution for dual MIMO systems in Ricean fading," *IEEE Commun. Lett.*, vol. 8, no. 1, pp. 18–20, Jan. 2004.

[18] The Wolfram functions site. Wolfram Research, Inc. [Online]. Available: http://functions.wolfram.com

[19] I. Gradshteyn and I. Ryzhik, *Table of Integrals, Series, and Products*, 7th ed. Academic Press, 2000.

[20] Z. Wang and G. Giannakis, "A simple and general parameterization quantifying performance in fading channels," *IEEE Trans. Commun.*, vol. 51, no. 8, pp. 1389–1398, Aug. 2003.

[21] J. Winters, J. Salz, and R. Gitlin, "The impact of antenna diversity on the capacity of wireless communication systems," *IEEE Trans. Commun.*, vol. 42, no. 234, pp. 1740–1751, Feb. 1994.